Biosensors and Bioelectronics 49 (2013) 53–62

Contents lists available at SciVerse ScienceDirect

Biosensors and Bioelectronics

journal homepage: www.elsevier.com/locate/bios

Template-directed hierarchical self-assembly of graphene based hybrid structure for electrochemical biosensing

Onur Parlak [a], Atul Tiwari [b], Anthony P.F. Turner [a], Ashutosh Tiwari [a,*]

[a] Biosensors and Bioelectronics Centre, Department of Physics, Chemistry and Biology (IFM), Linköping University, 581 83 Linköping, Sweden
[b] Hawaii Corrosion Laboratory, Department of Mechanical Engineering, University of Hawaii at Manoa, 96822 HI, USA

ARTICLE INFO

Article history:
Received 4 March 2013
Received in revised form
3 April 2013
Accepted 5 April 2013
Available online 23 April 2013

Keywords:
Hierarchical self-assembly
Template directed hybrid nanomaterial
Graphene
Nano-biointerface
Biosensor

ABSTRACT

A template-directed self-assembly approach, using functionalised graphene as a fundamental building block to obtain a hierarchically ordered graphene–enzyme–nanoparticle bioelectrode for electrochemical biosensing, is reported. An anionic surfactant was used to prepare a responsive, functional interface and direct the assembly on the surface of the graphene template. The surfactant molecules altered the electrostatic charges of graphene, thereby providing a convenient template-directed assembly approach to a free-standing planar sheet of sp^2 carbons. Cholesterol oxidase and cholesterol esterase were assembled on the surface of graphene by intermolecular attractive forces while gold nanoparticles are incorporated into the hetero-assembly to enhance the electro-bio-catalytic activity. Hydrogen peroxide and cholesterol were used as two representative analytes to demonstrate the electrochemical sensing performance of the graphene-based hybrid structure. The bioelectrode exhibited a linear response to H_2O_2 from 0.01 to 14 mM, with a detection limit of 25 nM ($S/N=3$). The amperometric response with cholesterol had a linear range from 0.05 to 0.35 mM, sensitivity of 3.14 μA/μM/cm^2 and a detection limit of 0.05 μM. The apparent Michaelis–Menten constant (K_m^{app}) was calculated to be 1.22 mM. This promising approach provides a novel methodology for template-directed bio-self-assembly over planar sp^2 carbons of a graphene sheet and furnishes the basis for fabrication of ultra-sensitive and efficient electrochemical biosensors.

1. Introduction

A range of nanoscale carbon-based building blocks, including nanotubes (Xia et al., 2003), graphite (Novoselov et al., 2004), fullerenes (Liu et al., 1998) and graphene (Stankovich et al., 2006), have attracted significant interest due to their extraordinary physical and chemical properties. Recently, research focused on graphene has advanced rapidly as this extraordinary material has become the preferred alternative to provide high surface area, high electrical conductivity, strong mechanical strength, biocompatibility and low manufacturing cost (Chen et al., 2008; Li et al., 2009). The extension of long range π-conjugation over the whole structure makes graphene a unique material for biosensors (Schedin et al., 2007; Shan et al., 2010), chemical sensors (Robinson et al., 2008), energy storage devices (Sofo et al., 2007), field effect transistor (Zhang et al., 2009), light emitting devices (Bonaccorso et al., 2010) and transparent, flexible, conductive polymer nanocomposite applications (Chen et al., 2011; Wang et al., 2008). Graphene-based materials are now being used widely in electroanalytical research for electrochemical sensing and immobilisation of biomolecules with high sensitivity and selectivity.

The biocompatibility and excellent electron transfer properties of graphene pave the way for its use in chemical and biological sensing (Lu et al., 2009). Covalent interactions are mostly obtained by doping or by chemical reaction with the functional groups which are formed during the synthesis of graphene (Veca et al., 2009). The former approach partly destroys the graphene conjugation system and results in suppression of its intrinsic properties. However, non-covalent interactions *via* van der Waals forces, electrostatic attraction, hydrogen bonding, coordination bonds or $\pi \rightarrow \pi$ stacking interactions mostly preserve the natural properties of graphene. In addition, although non-covalent bonds may be weak compared to covalent interactions, it is well-known, especially in biological systems, that multiple non-covalent bonds can provide quite enough stability for post-functionalisation (Liu et al., 2012). Recently, Li et al. showed that horseradish peroxidase can easily be assembled under physiological conditions on surfactant-modified graphene to yield high stability and sensitivity (Zeng et al., 2010). It is also known that assembly of gold nanoparticles into a graphene–enzyme structure increases electron transfer and the effective surface area of bioelectrodes (Lambert et al., 2009). The driving force for gold nanoparticle assembly is the interaction between the hydrophilic graphene surface and the gold

* Corresponding author. Tel.: +46 13 28 2395; fax: +46 13 13 7568.
E-mail addresses: ashutosh.tiwari@liu.se, ashunpl@gmail.com (A. Tiwari).

0956-5663/$ - see front matter © 2013 Elsevier B.V. All rights reserved.
http://dx.doi.org/10.1016/j.bios.2013.04.004

nanoparticles. The functional and large surface area of graphene should be a promising building block for hybridisation with gold nanoparticles. To date, only a few studies on graphene/gold nanoparticle assembly have been reported *via* the self-assembly approach, based on π–π stacking interactions and electrochemical interaction for sensing applications (Fang et al., 2010). Uniform distribution and sufficiently high loading are still challenges to be overcome. Herein, we describe a self-assembled structure containing functionalised graphene–enzyme and gold nanoparticles to deliver high sensitivity for cholesterol sensing, accelerated electron transfer and good retention of enzyme activity.

The self-assembly approach has been widely used to produce more efficient and more functional materials (Mirkin et al., 1996; Sanchez et al., 2005). With an appropriate design, self-assembled hybrid structures can deliver synergistic effects, resulting in highly desirable materials with advanced performance. The forces behind the thermodynamic equilibrium state can be manipulated by conventional chemistry or more specifically directed by using templates or applying external fields. In order to achieve directed self-assembly, the base constituent should be carefully chosen and molecular interactions tailored by its functionalisation while the whole process can be modulated in terms of thermodynamic forces. In this way, a new ordered equilibrium may be established within the whole self-assembled structure. Directional interactions are achieved by designing stimuli–responsive interfaces or specific physical properties, provided by post-functionalisation under external directing fields or in the presence of directing surfaces.

In this report, we focus on the template directed approach to construct a self-assembled structure. Template-directed assembly is defined as a process which modulates a self-assembled system using surface-modified one-dimensional, two-dimensional or three-dimensional materials having a functionalised surface suitable for additional assembly. Here, the surface-modified graphene was chosen as a model two-dimensional template. A straightforward method is described to assemble graphene with enzyme and gold nanoparticles by hierarchical structuring using electrostatic and hydrophilic interactions, respectively, for the fabrication of an enzyme electrode as illustrated in Scheme 1. The graphene plays a key role in the directed self-assembly by electrostatic and hydrophilic interactions. In the study, a negatively charged surfactant, sodium dodecyl benzene sulphonate (SDBS), has been employed to functionalise the graphene surface to not only assist the dispersion in aqueous media, but also to direct the self-assembly of both the enzyme and the metallic nanoparticles. Surfactant molecules on the graphene surface become the fundamental building blocks of the self-assembly structure that help to direct gold nanoparticles and enzyme molecules on the graphene template. As model enzymes, cholesterol oxidase and cholesterol esterase, which are positively charged in physiological media (pH 7.4), were chosen. It is shown that functionalised graphene and enzymes are spontaneously assembled into hierarchical structures due to electrostatic attraction. In other words, surface functionalisation directs enzyme molecules to assemble on the surface of the graphene, followed by gold nanoparticles as a third constituent of the assembled structure. Gold nanoparticle assembly on the surface of functionalised graphene was achieved via hydrophilic interactions. Thus, surfactant molecules create a hydrophilic environment on the highly hydrophobic graphene surface and direct hydrophilic gold particles on to the surface without any additional coupling chemistry.

For the proof of principle, we have chosen cholesterol oxidase and cholesterol esterase enzymes. Cholesterol and cholesteryl ester are two of the main constituents of all animal cells, and they are mostly present in the brain and nerve tissues (Dey and Raj, 2010; Kuila et al., 2011). The estimation of cholesterol in blood is a crucial step for controlling and early diagnosis of many life-threatening diseases, such as cerebral thrombosis, coronary heart disease, hypertension and Alzheimer. Various analytical techniques have been reported for monitoring cholesterol level in serum and food samples, including colorimetric (Li et al., 2011), spectrophotometric (Kumar et al., 2000) and non-enzymatic methods (Li et al., 2010). Electrochemical methods, however, offer simplicity, high sensitivity and low production costs (Gopalan et al., 2009; Tan et al., 2005). These may be enhanced by the use of nanoscaled materials such as this graphene–enzyme–nanoparticle hierarchical hybrid. Resulting novel self-assembled structures provide a larger electrochemically active surface for the adsorption of large amounts of enzymes and promote rapid electron transfer, resulting in ultra-sensitive and selective sensors.

2. Materials and methods

2.1. Chemicals

Cholesterol (≥99%), cholesteryl stearate (96%), cholesterol oxidase (ChEt) (≥50 units/mg, from *Brevibacterium* species),

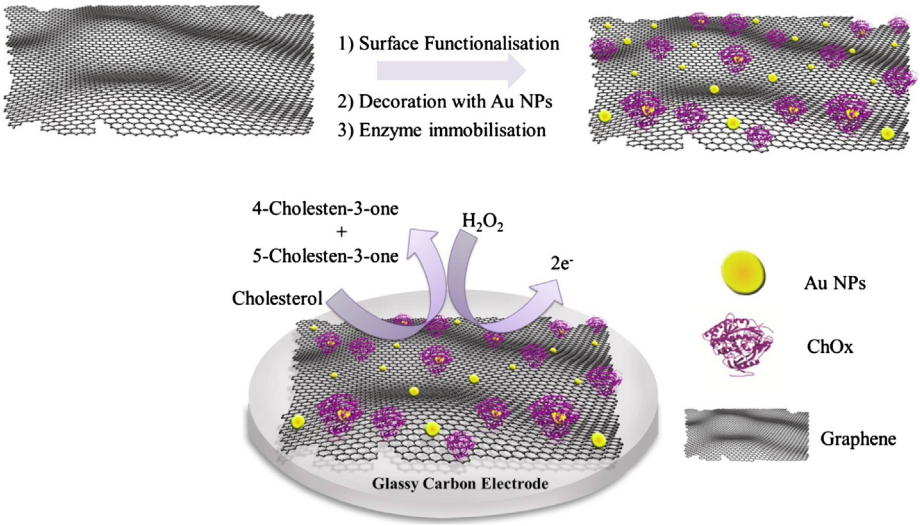

Scheme 1. Schematic representation of the self-assembled graphene–gold–enzyme hierarchical hybrid structures on glassy carbon electrode and sensing process on the electrode surface .

cholesterol esterase (ChOx) (from *Psedomonas fluorescens* species), peroxidase form horseradish (HRP) (300 units/mg), sodium dodecylbenzenesulfonate (SDBS), 4-aminoantipyrene (4-AAP) (≥99%), hydrogen peroxide (H_2O_2) (ACS reagent, 30 wt% in H_2O), phenol (≥99.5%), gold nanoparticles solution stabilised suspension in 0.1 M phosphate buffer solution (PBS) (10 nm diameter, reactant free), t-octylphenoxy polyethoxy ethanol (Triton X-100) (laboratory grade), chitosan, polyvinyl alcohol (PVA), potassium dihydrogen phosphate monobasic (KH_2PO_4) (99.99%), dipotassium hydrogen phosphate (K_2HPO_4) (≥99%), potassium chloride (KCl) (≥99%), potassium ferrocyanide ($K_3[Fe(CN)_6]$) (≥98.5%), and potassium ferricyanide ($K_4[Fe(CN)_6]$) were purchased from Sigma-Aldrich (St. Louis, MO, USA) and were used without further purification. PBS (0.1 M, pH 7.4) and ferri/ferro-cyanide solutions were used as supporting electrolyte for all amperometric measurements. Aqueous solutions were prepared with double-distilled water from Millipore system (18.2 MΩ cm).

2.2. Synthesis of graphene nanosheets

Graphite oxide was prepared by adopting the modified Hummers method (Hummers and Offeman, 1958). The ACS grade sulphuric acid (H_2SO_4) (46 mL) was pre-cooled to 0 °C in an ice-bath for 30 min followed by the addition of 2.0 g graphite powder. Mixture was stirred for 30 min and 6.0 g of potassium permanganate ($KMnO_4$) was added gradually. The temperature of the reaction bath was increased to 35 °C and the reaction mixture was stirred until grey coloured semi-solid paste was obtained. The reaction mixture was brought to room temperature and left undisturbed. Water (92 mL) was then added slowly to the above paste and the content was stirred slowly for 30 min. Viscous liquid was then added to a copious amount of pure water followed by vigorous stirring. 10 ml 30% hydrogen peroxide was added to this solution that immediately turned the colour of the solution from grey to yellow. Functionalised graphite solution was then filtered through a sintered/fritted glass funnel and washed several times with dilute hydrochloric acid (HCl) solution until neutral pH was obtained. Finally, the content was isolated using a high speed centrifuge. The semi-solid content was dried in flowing air. This dried semi-solid content was taken in a quartz round bottom flask. Argon gas was passed in the flask for 15 min and the content was thermally shocked for 15–30 s at 1100 °C. The dry solid black powder graphene was obtained.

2.3. Preparation of graphene based hierarchically self-assembled hybrid structures

In a typical preparation of graphene based self-assembled nanoconjugates, 1.0 mg of as-synthesised graphene was dispersed in 5 mL of 0.1 M SDBS aqueous solution. The reaction mixture was sonicated for 1 h, and mixed for 3 h at room temperature (RT) under mild stirring. After 3 h reaction time, the resulting suspension was subjected to three cycles of centrifugation to isolate surface-capped graphene nanosheets. The graphene nanosheets were washed with distilled water to remove excess SDBS and dried at RT prior to bioconjugation with cholesterol oxidase and cholesterol esterase enzymes.

For bioconjugation of cholesterol oxidase/esterase enzymes with surface-modified graphene, 1.0 mg of cholesterol oxidase and 0.5 mg of cholesterol esterase were dissolved in 1 ml of PBS solution (0.1 M, pH 7.4), and the mixture was incubated for 3 h at 4 °C. The mixture was then centrifuged at 5000 rpm for 30 min, and the supernatant of the solution was collected for the determination of enzyme loading efficiency. The precipitate was washed with PBS and centrifuge successively three times to remove loosely attached enzymes from graphene surface. Same experiments were performed for different concentrations of graphene and enzyme with different pH values to determine enzyme loading efficiency.

As a last constituent, gold nanoparticles were assembled onto the graphene–enzyme conjugates. The standard for the addition of gold nanoparticles to structures was as follows: 1 mg of graphene–enzyme solids were re-dispersed in 1 ml of 0.1 M PBS solution containing 10 nm diameter gold nanoparticles (40 μg mL^{-1}). The mixture was incubated at 4 °C for 3 h to achieve a high amount of assembled gold nanoparticles onto to the eventual graphene–enzyme conjugate. The resulting suspension was isolated by centrifugation at 5000 rpm for 30 min and rewashed several times with PBS buffer to remove unassembled gold nanoparticles. Indeed, the supernatant of this solution was kept separately in order to calculate gold-assemble efficiency in the eventual conjugate. The product was then collected and stored in 0.1 PBS buffer at 4 °C for further use. The other conjugates, such as with/without gold or with/without enzyme, were prepared following the same procedures described above.

2.4. Determination of graphene–ChOx immobilisation efficiency

The immobilisation efficiency of cholesterol oxidase enzyme was determined indirectly by taking the amount of free enzyme in supernatant solution from the weight of added enzyme. The activity of free enzyme which was collected from supernatant solution was calculated according to the literature (Kumar et al., 2000). In each run, a constant amount of graphene (1.0 mg mL^{-1}) was used with respect to the different amount of cholesterol oxidase enzyme (from 0.1 mg to 3.5 mg).

2.5. Fabrication of bioelectrodes

Prior to immobilisation of the self-assembled enzyme–graphene based structure, glassy carbon electrodes (GCE) were carefully polished with 1, 0.3 and 0.5 μm α-alumina slurry successively then washed with deionised water. The bioconjugate solution (10 μL), which contained surface modified graphene–enzyme and gold nanoparticles, was mixed with 5 μL chitosan/PVA (3:1; mL) aqueous solution (1 wt% acetic acid) at 4 °C. The solution was sonicated for 5 min to achieve homogeneous dispersion. This suspension (15 μL) was drop-cast onto the GCE surface and dried for 8 h at 4 °C. The other electrodes, such as with/without gold or with/without enzyme, were prepared by the same procedures described above.

2.6. Instrumentation

The zeta potential of graphene dispersions was determined using a Nano ZS dynamic light-scattering (DLS) Zeta potential instrument (Malvern Instruments, Worcestershire, UK). Absorptions of all self-assembled structure in PBS solution were measured with a Cary 50 UV–vis Spectrometer (Varian). The resolution of the spectrophotometer was 1.5 nm and the photometric accuracy was ±0.01 in absorption. Transmission electron microscopy (TEM) was performed using a G^2 Spirit/Biotwin (FEI-Technai, Hillsboro, OR, USA) with a working voltage of 120 kV. Scanning electron microscopy (SEM) was performed using LEO 155 Gemini (Zeiss, OR, USA). FTIR measurements were carried out using a PE 100 FTIR spectrometer (PerkinElmer, Waltham, MA, USA). All the voltammetric and amperometric measurements were carried out with Ivium Stat.XR electrochemical analyser (Eindhoven, Netherlands). Impedance measurement was carried out with an Autolab potentiostat–galvanostat. A three-electrode cell with a glassy carbon (GC) working electrode, having 0.07 cm^2 surface area, and platinum wire auxiliary and Ag/AgCl (3 M KCl) reference

electrodes were used in the voltammetric and amperometric measurements.

3. Results and discussion

Scheme 1 represents the overall process for the preparation of graphene-based hierarchically self-assembled hybrid structures for electrochemical sensing. The synthesis strategy is, first, to obtain surface-modified graphene via non-covalent interaction with an anionic surfactant. This is one of the crucial steps to achieve free-standing and stable graphene dispersions for further assembly on the surface. The second step involves the conjugation of the enzyme with surface-modified graphene and the gold assembly. Then, a hierarchically self-assembled dispersion is cast on the electrode surface after pre-assembling cationic chitosan-*g*-poly(vinyl alcohol).

3.1. Preparation and characterisation of hierarchically self-assembled graphene nanostructures

It is well-known that chemically reduced graphene nanosheets are highly hydrophobic in nature (Kim et al., 2010) and tend to be aggregated and stacked irreversibly with each other in colloidal medium. In order to prevent such an aggregation and sustain their unique chemical and physical properties, non-covalent surface modifications methods have the potential to manipulate the surface properties by changing the pH and temperature (Liu et al., 2012).

In order to obtain more stable and functional nanostructures, the surface of graphene was modified by using an anionic surfactant, SDBS. As a member of linear alkyl sulphonates, it contains long alkyl chain (dodecyl-$C_{12}H_{25}$), which gives its hydrophobic nature and a benzenesulphonate ($C_6H_5SO_3^-$) group which is responsible for its hydrophilic character. Firstly, partially reduced hydrophobic graphene powder (1.0 mg) was dispersed in a 5 mL aqueous solution containing 0.1 M SDBS and sonicated to produce a well-dispersed state. In previous trials, although low concentrations of SDBS (0.01 and 0.05 M) gave homogeneous dispersions, long-term stability could not be achieved due to the lack of enough surface charge density (Fig. S5, Supporting information). In addition, long sonication time (≥5 h) also destroyed the sheet-like structures of graphene, changed the morphology and resulted in particle-like graphene structures (50–60 nm) (Fig. S4, Supporting information) (Li et al., 2012).

Fig. 1a and b shows SEM images of graphene sheets before and after surface modification, respectively. It is clear that, surface-modified graphene sheets are in the well-separated form compared to the unmodified one. Conversely, unmodified graphene had much thicker edges and a high tendency for stacking. The insets in each panel also show the stability of the dispersions visually. The solution containing unmodified graphene nanosheets did not show any homogeneity even after 30 min in pure water and settled down immediately after sonication. However, the solution containing modified graphene sheets seemed to be more stable and homogeneous.

The surface charge of the colloidal system is one of the key parameters that not only defines stability of dispersion, but also allows us to characterise electrochemical equilibrium on the interface. In the present system, graphene nanosheets were functionalised with SDBS through hydrophobic–hydrophobic interaction between alkyl chain of surfactant and the basal plane on the graphene surface. Another interaction might be partially hydrophilic interaction between sulphonic groups (polar groups) and carboxyl groups in the graphene basal plane. The graphene nanosheets are dispersed in an aqueous solution by the help of these interactions, surface groups of graphene and adsorbed anions turn out a surface charge. The surface charge generates electrical potential due to the electrostatic repulsive force that exists between the modified graphene surface and the medium by depending on the zeta potential. In addition to the colloidal stability of the dispersion, the zeta potential value also provides qualitative (sign) and quantitative (magnitude) information about the effective surface charge related to the electrical double layer around the surface. The isoelectronic point (IEP), which is described as the pH at which the surface is neutrally charged, can also be derived from the zeta potential measurement. The zeta potential of graphene nanosheets before and after surface modification by SDBS were measured to explore the dispersion quality and charge characteristics at different pH values, as shown in panel (c) of Fig. 1. Zeta potential values of unmodified graphene decreased from +12 to −22 mV. Based on zeta potential values, it is clear that chemically reduced graphene nanosheets cannot be considered as completely reduced based on zeta potential values. Due to the presence of carboxylic acid functionality (–COOH) on the surface, little charge variation from positive to negative results as pH increases due to the deprotonation of the surface groups. These carboxylic acid functionalities dissociate and form carboxyl groups ($–COO^-$) which make the surface of graphene more negative even though there are no extra charged ions on the surface. Although there is relatively high level of negative charge on the surface, they are not enough to obtain a homogeneous and stable dispersion over a wide range of pH values. However, SDBS-modified graphene shows more stability and homogeneity over a wide range of pH. The optimum surface charge of graphene was obtained by varying concentration of surfactant during surface modification (Fig. S5, Supporting information). The zeta potential measurements of these dispersions were performed after re-dispersion into aqueous solution. On the basis of dispersion, 0.1 M SDBS was chosen as the optimum concentration to achieve a stable and functional surface. It was relatively stable over a range of pH values (pH 6–10) with low zeta potential values (−28 to −40 mV). It was also found that when the SDBS concentration of the aqueous solution increases, the isoelectronic point of the surface (IEP) shifts to that of the lower pH values. The partially reduced nature of the graphene surface and the presence of negatively charged $–COO^-$ functionality may cause repulsion of negatively charged anionic surfactant molecules via coulombic interactions between the two negative sides thereby shifting the EIP to lower pH values. These measurements show that SDBS is a good dispersant in terms of delivering a zeta potential in the range from −28 to 50 mV, even at relatively low concentrations.

In order to prepare hierarchically self-assembled graphene based composites the graphene surface was first functionalised with anionic surfactant to produce a negatively charged graphene surface in well-dispersed solution. In the second step, enzyme and nanoparticles were assembled on the functionalised graphene surface *via* electrostatic and hydrophilic–hydrophilic interactions, respectively. As a model system, cholesterol oxidase enzyme was chosen. Due to the positive surface charge of this enzyme in physiological media (pI=4.7), self-assembled structures could be easily achieved through electrostatic attractions as in layer-by-layer methodology. To incorporate gold nanoparticles into the self-assembled system *via* hydrophilic–hydrophilic interaction, graphene–enzyme solution was centrifuged and re-dispersed in 0.1 M PBS solution containing 10 nm gold nanoparticles (mg mL^{-1}).

The hybrid structures prepared as a hierarchical self-assembly were examined by SEM and TEM as shown in Fig. 2a–d. The samples were prepared by dropping 10 μg of each solution and cast on a TEM grid. The inset of Fig. 1a represents a typical TEM image of the as-prepared graphene nanosheet, in which the sheet displays wrinkled structure and high surface area without any stacking. It shows that this graphene is suitable for colloidal surface-modification and enzyme immobilisation. Fig. 1a and b

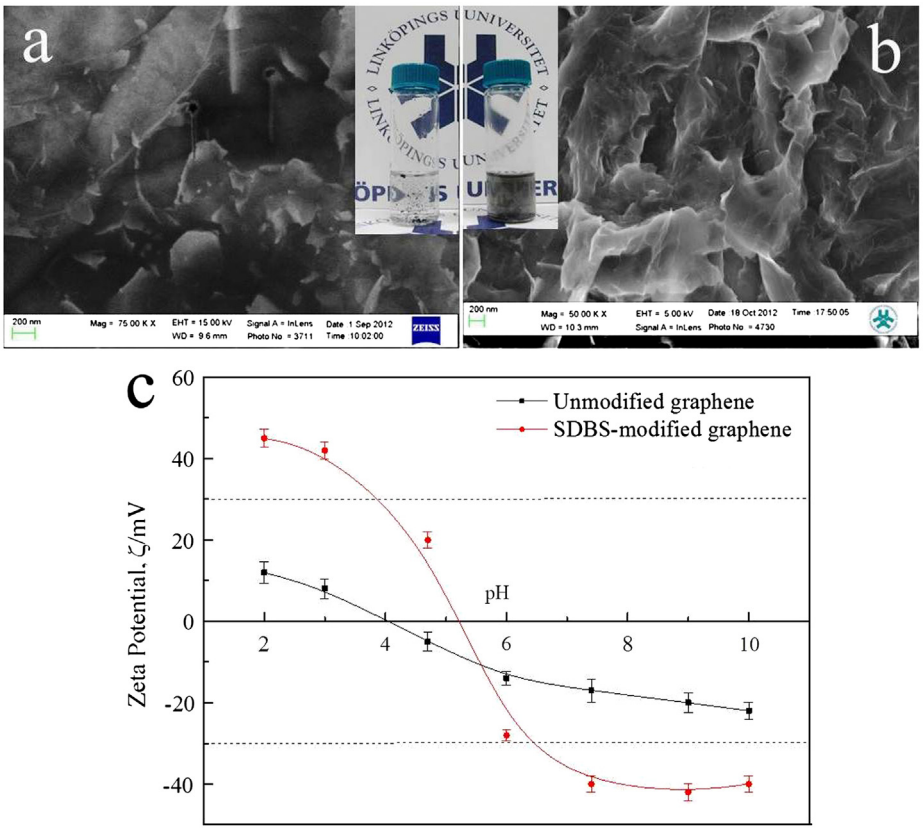

Fig. 1. SEM images of graphene nanosheets before (a) and after (b) surface functionalisation. Zeta potential measurement of graphene at various pH values before and after surface modification (c). Inset: photographic images of dispersions prepared with unmodified and modified graphene sheets in PBS solution.

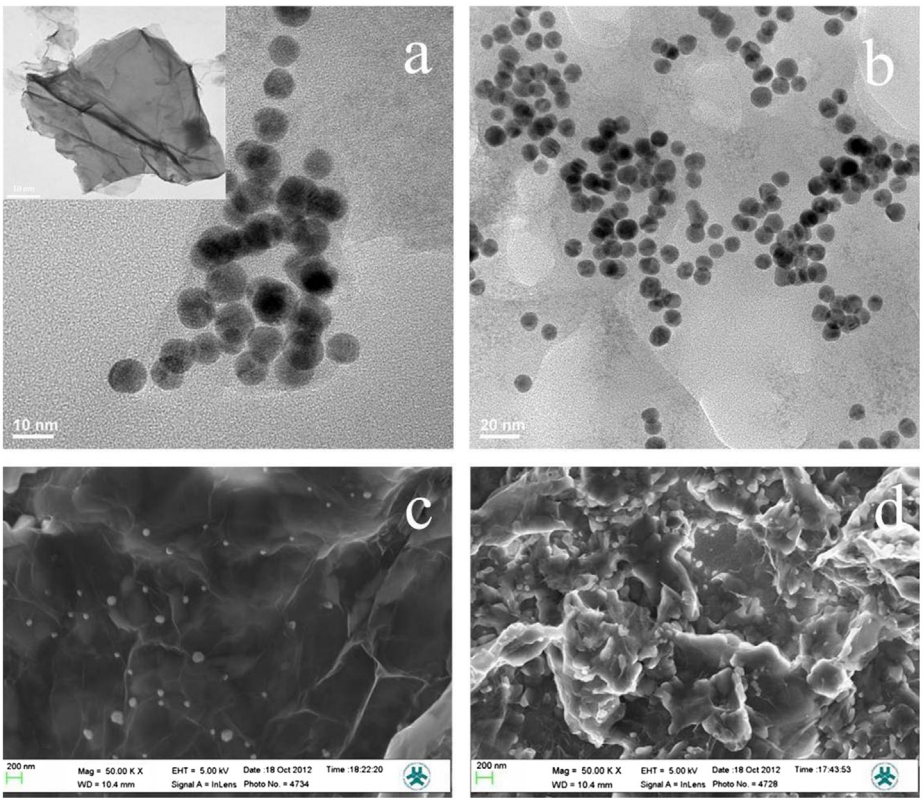

Fig. 2. TEM images of enzyme and gold assembled structures (a) and (b). SEM images of graphene–gold nanoparticles (c) and graphene–enzyme–gold nanoparticle self-assembled structures (d). Inset: TEM image of unmodified graphene.

shows TEM images of the graphene–enzyme–gold assembly. As can be seen in these figures, gold nanoparticles are selectively and homogeneously assembled on graphene surface without any self-condensation and aggregation. A higher magnification of Fig. 1c can be seen in the supporting figure (Fig. S3, Supporting information). In this image, all particles are well-ordered single crystals with an appropriate fringe distance corresponding to the lattice plane of gold. Although higher magnification of graphene–enzyme–gold nanoparticles (Fig. 1b) shows good homogeneity and dispersion, it is difficult to identify enzyme structures in these images. Notably, in some graphene–enzyme conjugation studies, dark spots on graphene surface have been attributed to the enzyme structures (Zeng et al., 2010); it is apparent that more images of such an enzyme–graphene conjugate are necessary to comment more precisely (Fig. S3, Supporting information). It is worth mentioning that the presence of enzyme structures on the graphene surface was proven in our case by using electrochemical and enzyme activity assay experiments as described in proceeding section. The SEM images of graphene–gold and graphene–enzyme–gold nanoparticle assemblies are shown in Fig. 2c and d, respectively. In panel (c), gold nanoparticles on the graphene surface were seen in a well-dispersed state, although their sizes were not uniform throughout the structures. There is a low degree of aggregation that could be due to the centrifugation process during the preparation. In the graphene–enzyme–nanoparticle assembly, enzymes and gold nanoparticles can be seen on the surface of the graphene. Homogeneous dispersion has been achieved on the surface of graphene not only for the gold nanoparticles, but also for the enzyme molecules. The surface modification provides a more accessible surface for enzyme attachment and generates a flexible surface structure which can comply with the enzyme molecules with the help of electrostatic self-assembly.

In order to calculate enzyme immobilisation efficiency, an enzyme activity assay was performed according to the literature (Allain et al., 1974). Enzyme loading efficiencies on the surfactant-modified graphene surface with respect to enzyme concentration and pH are shown in Fig. 3a and b, respectively. The enzyme loading efficiency test (Fig. 3b) with different concentrations of enzyme was conducted at pH 7.4. Enzyme loading shows a linear correlation from 0.1 mg to 1.5 mg, indicating 100% loading efficiency. With enzyme concentrations of 2.0, 2.5 and 3.0 mg, loading efficiency reduced to 87.5%, 80% and 70%, respectively. The surface of graphene was saturated above 3.0 mg enzyme due to the steric hindrance. The effect of pH on the enzyme loading efficiency is shown in Fig. 3b. Immobilisation was pH dependent and involved electrostatic attraction between the enzyme and surfactant molecules on the surface of graphene. The surface modification of graphene created a tunable surface whereby the immobilisation efficiency can be controlled by varying the pH of the reaction medium. For example, at pH 4, the graphene surface is positively charged and the immobilisation efficiency was about 72%; this reduced to its lowest value at pH 4.7, which is the EIP of cholesterol oxidase. At this pH, the enzyme is neutral while the graphene surface is still positively charged. Almost the same loading efficiency was obtained at pH 5.2, which is the IEP of graphene surface and the enzyme has a positively charged surface. In this pH range (pH 4–5.2), immobilisation might be provided by hydrophobic–hydrophilic interactions. Electrostatic attraction becomes dominant at pH values above 5.5 because the surface charge of graphene turns negative and enzyme is positively charged. The highest loading efficiency was achieved at pH 7.4, which is also the most stable point of the graphene dispersion. Here, 100% loading was obtained, after which it declined to 90% at pH 10. It can be inferred from these results that electrostatic attraction is the dominant force for immobilisation efficiency and can be controlled by changing the pH of the reaction medium.

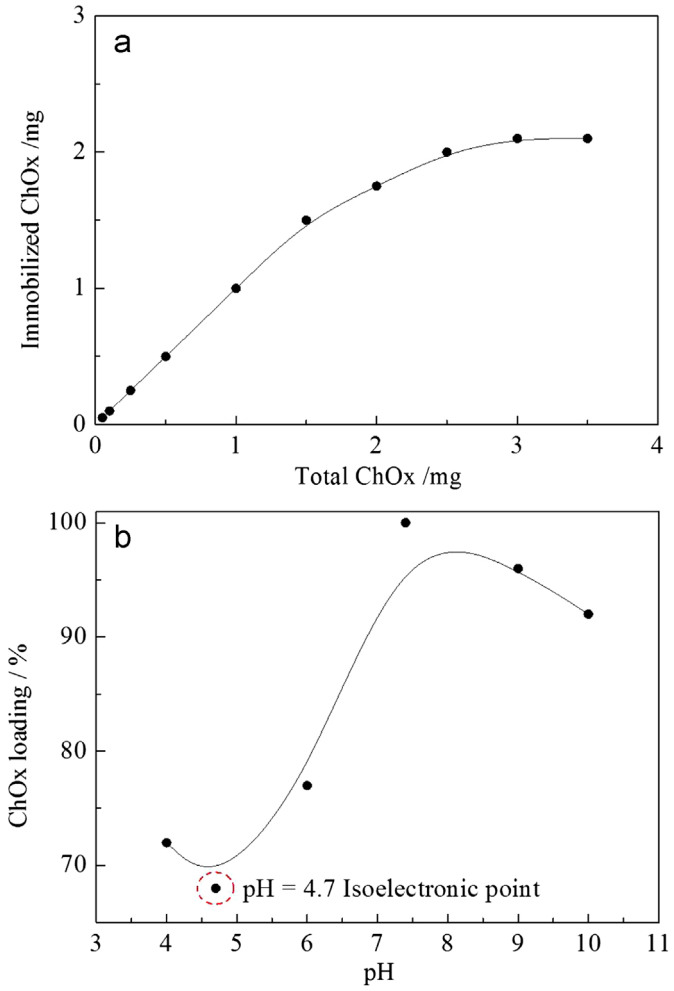

Fig. 3. Enzyme loading on functionalised graphene as a function of total amount of enzyme (a). Effect of enzyme loading on the graphene surface with various pH values (b).

3.2. *Electrochemical properties of hierarchically self-assembled graphene-modified electrodes*

The electrochemical properties of all modified electrodes were characterised by measuring voltammetric and electrochemical impedance (EIS) responses in 0.1 M PBS solutions containing 5 mM $Fe(CN)_6^{3-/4-}$ and 0.1 KCl. The results were shown in Fig. 4a and b and Figs. S7 and S8 (Supporting information). The CV analysis of the redox reaction of $Fe(CN)_6^{3-}$ and $Fe(CN)_6^{4-}$ is a well-known method to characterise electrochemical behaviour of modified and bare electrodes and the simplest way to determine electron transfer rate (Unnikrishnan et al., 2013). The CV responses of all modified electrodes displayed a classical sigmoidal shape with different peak-to-peak potential separations. The larger peak separation indicated slow electron transfer kinetics (Nugent et al., 2001). All electrodes containing graphene-based assemblies and chitosan/PVA polymeric mixtures showed narrow peak-to-peak separations, indicating that fast electron transfer was achieved for each electrode. The polymer modified GCE (without any graphene-based assembly) also showed exceedingly narrow ΔE_p value around 100 mV, which indicates a faster electron transfer rate compared to the more commonly used negatively charged Nafion polymer, which is most widely used in electrochemical devices as a binder (Hrapovic et al., 2004). The relatively narrow peak separation for the chitosan/PVA-modified GC electrode could be due to the poly-anionic character of this polymer mixture on the

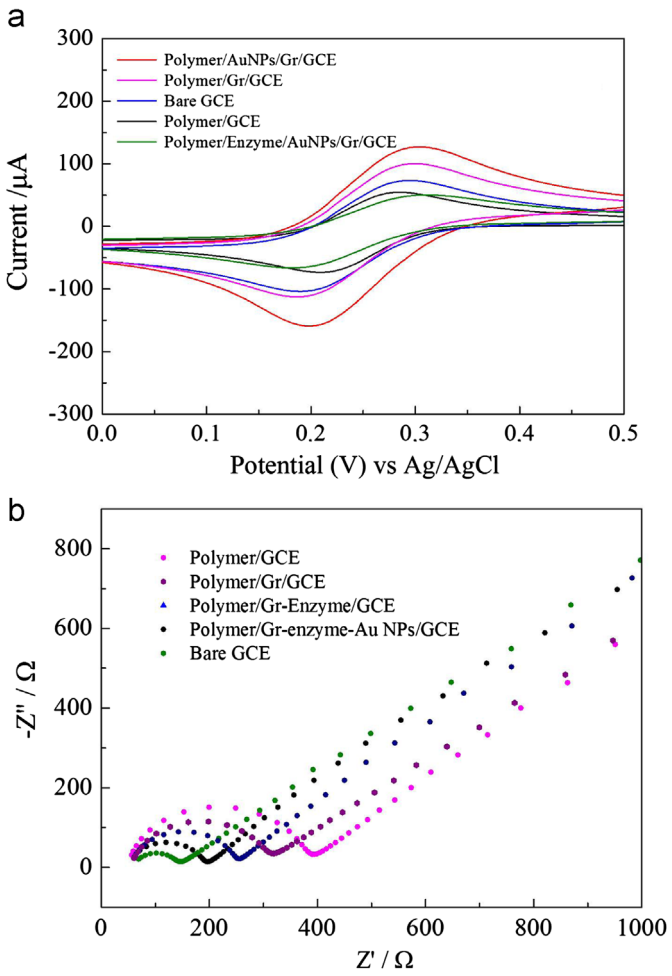

Fig. 4. Cyclic voltammetric (a) and impedance (b) response of bare and modified electrodes in 5 mM $Fe(CN)_6^{4-}$ and 0.1 M PBS at 50 mV s^{-1} vs. Ag/AgCl reference electrode. The inset in (b) is the equivalent circuit used to fit the data.

surface of electrode enhancing electron transfer between its positive charges and the negatively charged ferrocyanide. After modification of the electrode surface with graphene–gold nanoparticle assembly, the peak current of $Fe(CN)_6^{3-/4-}$ increased relative to electrodes modified only with graphene, indicating that the incorporation of nanoparticles played a decisive role in creating a higher electroactive surface area and providing the conductive interlayer for the electron transfer of $Fe(CN)_6^{3-/4-}$. Moreover, when the peak currents and ΔE_p of modified electrodes are compared, it is clear that the presence of gold nanoparticles in the assembled system enhances the electron transfer. The graphene–gold nanoparticle/CHIT/PVA polymer assembly has narrower peak-to-peak separation (80 mV) than its graphene/CHIT/PVA counterpart (140 mV).

The effect of scan rates on the cathodic (I_{pc}) and anodic peaks (I_{pa}) of graphene–enzyme–gold nanoparticle self-assembled structure immobilised GC electrode together with polymer mixture is shown in Fig. S7 (Supporting information). Both anodic and cathodic peak currents increased linearly with increasing scan rates (10–100 mV s^{-1}), which suggest a typical diffusion-controlled electrode process. The scan-rate dependence of both anodic and cathodic peak currents and the respective linear regression equations are shown in Fig. S7 (Supporting information).

The electron transfer properties of electrodes with different graphene based self-assembled structures were further characterised by electrochemical impedance spectroscopy (EIS). The Randles circuit was chosen to fit the impedance outputs (inset of Fig. 4b). The results are shown as Nyquist plots of spectra which contain semi-circular and linear portions (Fig. 4b). The plot indicates both electron transfer limited (semi-circular portion) and diffusion processes (linear portion) occurring at the same time. The charge transport resistance (R_{CT}) at the electrode surface can be quantified based on the diameter of the semi-circular part of plot and described by the following equation (Chang and Park, 2006):

$$Z_{(\omega)} = R_s + \frac{R_{CT} + \sigma\omega^{-1/2}}{(C_d\sigma\omega^{1/2}+1)^2 + \omega^2 C_d^2 (R_{CT} + \sigma\omega^{-1/2})^2} - j\frac{\omega C_d (R_{CT} + \sigma^{-1/2})^2 + \sigma\omega^{-1/2}(\sigma\omega^{1/2} C_d + 1)}{(C_d\sigma\omega^{1/2}+1)^2 + \omega^2 C_d^2 (R_{CT} + \sigma\omega^{-1/2})^2} \quad (1)$$

where R_s is the solution resistance, C_d is the double layer capacitance, ω is the $2\pi f$, where f is the frequency, and σ is defined as

$$\sigma = \frac{RT}{\sqrt{2}F^2 A}\left(\frac{1}{\sqrt{D_o}C_o^*} + \frac{1}{\sqrt{D_R}C_R^*}\right) \quad (2)$$

where A is the area of the electrode, and D_o and D_R are the diffusion coefficients of oxidant and reductant, respectively. C_o and C_R represent the bulk concentrations of oxidant and reductant, respectively. According to calculation, R_{CT} of CHIT/PVA mixture modified electrode was found as 425 Ω which is higher than bare GCE (59 Ω). Thus, the presence of polymer layer on the surface of the electrode hinders the electron transfer. However, when the chitosan–PVA matrix was mixed with graphene, the R_{CT} values decreased to 130 Ω. This shows that graphene improves the conductivity and the electron transfer process. Moreover, when the graphene–gold nanoparticle assembly was mixed with the polymer mixture, electron transfer resistance decreased to 97 Ω. Presence of gold nanoparticles on the graphene surface enhanced fast electron transfer kinetics. When enzyme-based graphene–enzyme–gold nanoparticle assembled structure was adsorbed on the electrode surface together with chitosan/PVA mixture, slight inhibition of electron transfer of the redox couple (189 Ω) resulted, due to the insulating properties of enzymes.

3.3. Amperometric biosensing

Oxidase-based biosensors often rely on the determination of H_2O_2 produced by the enzymatic reactions. The amount of peroxide generated is readily detected electrochemically and is directly proportional to the amount of substrate in the corresponding sample (Behera and Raj, 2007). In the present study, the electrocatalytic properties of the graphene–gold nanoparticle assembly immobilised on electrode surfaces were investigated by amperometry. Cyclic voltammetry of graphene–gold nanoparticle assembly-modified electrodes was measured in the presence of H_2O_2 (Fig. S9, Supporting information). The voltammetric current was observed with increasing concentration of H_2O_2 from 0.01 mM to 20 mM at a potential of 0.6 V. The results show that the modified electrode lowered the detection potential for H_2O_2 compared to the bare glassy carbon electrode, which oxidised H_2O_2 only above +0.8 V (Chi and Dong, 1993).

Further electrochemical properties of the modified electrodes were investigated by chronoamperometry. Fig. 5a shows the typical amperometric responses of the graphene–gold nanoparticle self-assembly modified electrode for successive additions of H_2O_2 at an applied potential of +0.6 V. The electrode exhibited fast response times of just under 3 s to steady state. The calibration curve for modified electrode is shown in Fig. 4b. The linear range was 0.05–14 mM with a sensitivity of 124.57 ± 1.55 μA/μM/cm^2. The sensitivity was calculated by dividing the slope of the calibration curve by the surface area of the bare electrode

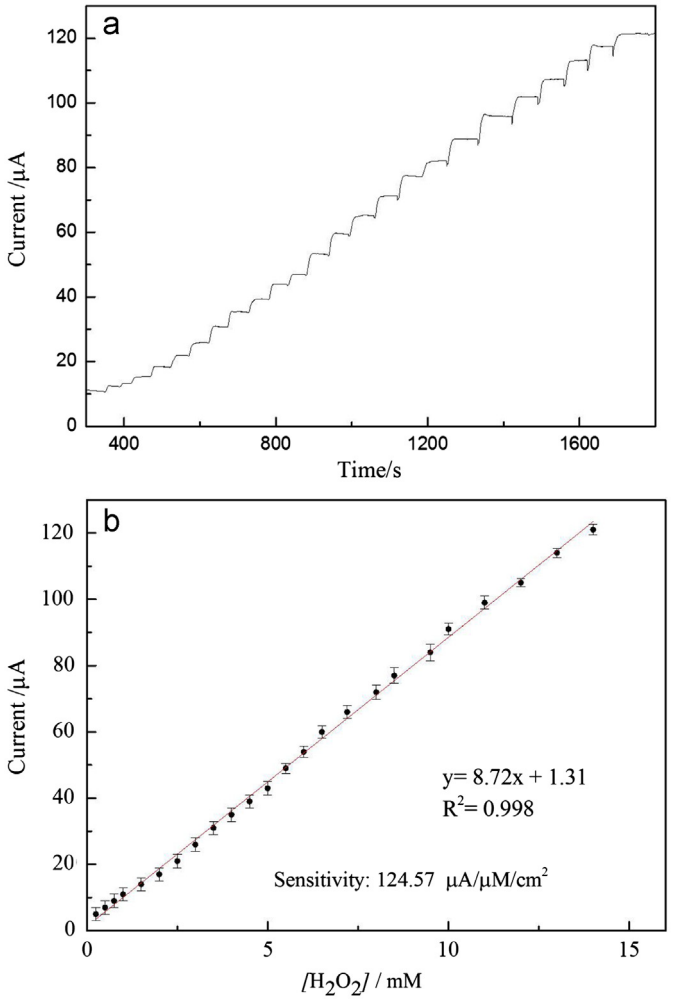

Fig. 5. Chronoamperometric response for the sensing of H_2O_2 with the graphene–gold nanoparticle structures modified electrode in phosphate buffer solution at 0.6 V vs. Ag/AgCl (a). Calibration curve of the graphene–enzyme–gold nanoparticle structures modified electrode corresponding to amperometric response at 0.6 V vs. Ag/AgCl in PBS (b).

(0.07 cm^2). The detection limit for this modified electrode was 25 nM ($S/N=3$). In order to see the effect of gold nanoparticles on the electrochemical process, electrodes were prepared with surface modified graphene and with immobilised gold nanoparticles alone. The chronoamperometric response of graphene and gold nanoparticle immobilised electrodes is shown in Fig. S11 (Supporting information) and the results of all three electrodes are summarised in Table 1. The typical amperometric response of the graphene and gold nanoparticle immobilised electrodes exhibited rather sluggish step increment compared to the graphene–gold assembled electrode. As shown in Table 1, the times to achieve steady-state current for these two electrodes were 10 s and 15 s, which were longer than those for the electrode with the fully assembled immobilised structure. The detection limits were calculated as 42 and 108 nM ($S/N=3$) and sensitivities were about 49.7 ± 1.25 and 32 ± 0.85 μA/μM/cm^2, respectively. On the basis of these results, functionalised graphene–gold nanoparticle electrodes exhibited better performance than both graphene that was only functionalised and gold nanoparticles alone. The enhancement in performance may be attributed to the homogeneous assembly of gold nanoparticles and the electrical properties of graphene materials. In addition, the strong adhesion between the surface of the gold nanoparticles and the C_π sites of the graphene basal plane appeared to favour electron transfer (Antolini, 2003).

Table 1
Detection limit, sensing range, sensitivity and response time of graphene–gold nanoparticle assembly, only graphene and only gold nanoparticle immobilised electrodes.

Base material	Detection limit[a] [μM]	Dynamic range[b] [mM]	Sensitivity[c] [μA/μM/cm^2]	Response time[d] [s]
Graphene/Au NPs	0.025	0.01–14	124.57 ± 1.55	3
Graphene	0.042	0.04–0.5	49.71 ± 1.25	10
Au NPs	0.108	0.04–0.16	32.00 ± 0.85	15

[a] Detection limits were calculated from the characteristic signal-to-noise ratio ($S/N=3$).
[b] Dynamic ranges were determined the linear portion of calibration curves.
[c] Sensitivities were obtained from the slopes of each calibration plots (concentration of H_2O_2 vs. current signal).
[d] Response times were determined when the currents reach to steady-state state at each addition of H_2O_2.

The highly sensitive electrode surface thus prepared was then combined with cholesterol esterase (ChEt). The polymer mixture and graphene-based self-assembled structure were mixed and cast on the electrode surface. In electrochemical cholesterol sensing, cholesterol and cholesteryl stearate are the substrates of ChOx and ChEt, respectively. The H_2O_2 generated in this process is subsequently oxidised at the electrode surface, producing the signal (Scheme 1).

$$\text{Cholestryl sterate} + O_2 + H_2O \overset{\text{ChEt}}{\Longrightarrow} \text{Cholestrol} + \text{Fatty acid}$$

$$\text{Cholestrol} + O_2 + H_2O \overset{\text{ChOx}}{\Longrightarrow} \text{Cholest} - 4\text{en} - 3\text{one} + H_2O_2$$

$$H_2O_2 \rightarrow 2H^+ + O_2 + 2e^-$$

Amperometric cholesterol sensing was performed using a three-electrode set-up and a working potential (0.6 V vs.Ag/AgCl). Calibration curves for both cholesterol and cholesteryl stearate were obtained by adding successive aliquots of increasing concentrations of cholesterol and cholestryl stearate and measuring the steady-state signal responses, which were achieved within 4 s. Fig. 6 shows the amperometric response and calibration curves obtained for the sensing of cholesterol and cholesterol ester. The calibration curve (Fig. 6c) is linear from 0.025 to 0.350 mM cholesterol at 0.6 V, and from 0.001 to 0.090 mM cholesteryl stearate (Fig. 6d) at the same applied voltage. The sensitivities for cholesterol and cholestryl sterate were 3.14 μA/μM/cm^2 and 2.57 μA/μM/cm^2, respectively. The detection limits were calculated as 0.05 μM and 0.22 μM (S/N=3) for cholesterol and cholestryl stearate, respectively. The novel biosensor had good reproducibility. The relative standard deviation (RSD) values of the current response to 0.1 mM cholesterol and cholesterol ester were 1.25 and 1.75, respectively, for three successive measurements at 0.6 V.

The apparent Michaelis–Menten constant (K_m^{app}) was calculated using a Lineweaver–Burk plot (Fig. S11, Supporting information) according to the following equation (Kamin and Wilson, 1980):

$$(1/I) = (K_m^{app}/I_{max})(1/C) + (1/I_{max}) \quad (3)$$

where I represents the steady-state current after addition of cholesterol. The maximum current (I_{max}) was determined at saturated level of cholesterol, and C is the concentration of cholesterol. The values of I_{max} and K_m^{app} were calculated by the analysis of the intercept and the slope of the plot and found to be 0.33 mA and 1.22 mM, respectively. The K_m^{app} value reflects the strong affinity between the enzyme and its substrate. The value obtained is much smaller than that reported in the literature for previous graphene-based cholesterol biosensors (Dey and Raj, 2010).

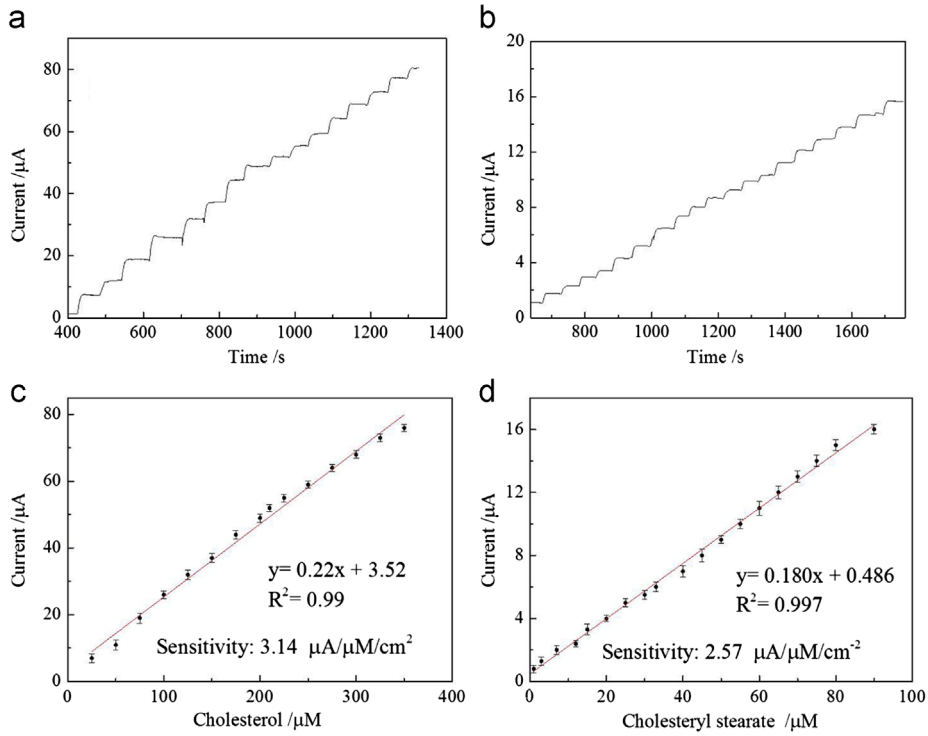

Fig. 6. Choronoamperometric responses for cholesterol (a) and cholesteryl stearate (b) at 0.6 V vs. Ag/AgCl in PBS. The calibration curves for cholesterol (c) and cholesteryl stearate (d) based on amperometric responses for (a) and (b), respectively.

The selectivity and specificity of the biosensor were evaluated in the presence of common interfering species such as ascorbic acid, uric acid and acetaminophen (paracetamol) in PBS solution. As shown in Fig. S12 (Supporting information), for each addition of 0.05 mM cholesterol, the biosensor showed a rapid response. However, no significant response was obtained on addition of 0.05 mM of uric acid, acetaminophen or ascorbic acid. This is presumably because the negative charge on the surface of the graphene effectively hinders the approach of negatively charged interfering species by electrostatic repulsion.

The biosensor showed better analytical performance than previously reported graphene-based cholesterol sensors on the basis of sensitivity, selectivity and response time. For instance, a cholesterol biosensor based on covalently attached graphene/enzyme conjugate, which was operated at a potential of −0.350 V, exhibited lower sensitivity (0.443 85 μA/μM/cm^2) for H_2O_2 and a higher detection limit (15 μM) (Manjunatha et al., 2012). A gold nanoparticle decorated graphene nanoplatelet based biosensor at 0.2 V potential showed narrower dynamic range (0.135 mM) and 0.314 μA/μM/cm^2 sensitivity (Aravind et al., 2011). A biosensor containing platinum–graphene hybrid structures exhibited lower detection limit (0.2 μM) and lower sensitivity value (2.07 μA/μM/cm^2). It is clear that, the currently reported biosensor has higher sensitivity, lower detection limits and faster response characteristics compared to previously reported graphene-based electrochemical biosensors.

4. Conclusion

In this study, we have developed a facile self-assembly approach to prepare hierarchically self-assembled graphene–enzyme–nanoparticle hybrids following a template-directed approach. As a template, graphene surface was functionalised by anionic surfactant. The surface modification of graphene was the driving force for the self-assembly process, which allowed us to generate a smart interface to control the assembly structure. The enzyme immobilisation on graphene surface was investigated under different pH values. The electrode showed a higher sensitivity and faster response time than any other reported study for a graphene-based cholesterol biosensor. Thereafter, hybrid structures were employed as an improved material for both H_2O_2 and cholesterol sensing, demonstrating wide linear range and low detection limits along with higher sensitivity. In contrast to previously reported graphene-based cholesterol biosensor approaches, the template directed self-assembly method provides an alternative for constructing hybrid structures with enzyme higher loading and uniform dispersion.

Acknowledgements

The authors wish to acknowledge the Swedish Research Council (VR-2011-6058357), the European Commission (PIIF-GA-2009-254955), and IGEN and LIST, the Linköping University for the generous financial support to carry out this research.

Appendix A. Supporting information

Supplementary data associated with this article can be found in the online version at http://dx.doi.org/10.1016/j.bios.2013.04.004.

References

Allain, C.C., Poon, L.S., Chan, C.S.G., Richmond, W., Fu, P.C., 1974. Clinical Chemistry 20 (4), 470–475.
Antolini, E., 2003. Journal of Materials Science 38 (14), 2995–3005.
Aravind, S.S.J., Baby, A.T.T., Arockiadoss, T., Rakhi, R.B., Ramaprabhu, S., 2011. Thin Solid Films 519 (16), 5667–5672.
Behera, S., Raj, C.R., 2007. Biosensors and Bioelectronics 23 (4), 556–561.
Bonaccorso, F., Sun, Z., Hasan, T., Ferrari, A.C., 2010. Nature Photonics 4 (9), 611–622.
Chang, B.Y., Park, S.M., 2006. Analytical Chemistry 78 (4), 1052–1060.

Chen, H., Muller, M.B., Gilmore, K.J., Wallace, G.G., Li, D., 2008. Advanced Materials 20 (18), 3557–3561.
Chen, Z.P., Ren, W.C., Gao, L.B., Liu, B.L., Pei, S.F., Cheng, H.M., 2011. Nature Materials 10 (6), 424–428.
Chi, Q.J., Dong, S.J., 1993. Analytica Chimica Acta 278 (1), 17–23.
Dey, R.S., Raj, C.R., 2010. Journal of Physical Chemistry C 114 (49), 21427–21433.
Fang, Y.X., Guo, S.J., Zhu, C.Z., Zhai, Y.M., Wang, E.K., 2010. Langmuir 26 (13), 11277–11282.
Gopalan, A.I., Lee, K.P., Ragupathy, D., 2009. Biosensors and Bioelectronics 24 (7), 2211–2217.
Hrapovic, S., Liu, Y.L., Male, K.B., Luong, J.H.T., 2004. Analytical Chemistry 76 (4), 1083–1088.
Hummers, W.S., Offeman, R.E., 1958. Journal of American Chemical Society 80 (6) 1339.
Kamin, R.A., Wilson, G.S., 1980. Analytical Chemistry 52 (8), 1198–1205.
Kim, J., Cote, L.J., Kim, F., Yuan, W., Shull, K.R., Huang, J.X., 2010. Journal of the American Chemical Society 132 (23), 8180–8186.
Kuila, T., Bose, S., Khanra, P., Mishra, A.K., Kim, N.H., Lee, J.H., 2011. Biosensors and Bioelectronics 26 (12), 4637–4648.
Kumar, A., Malhotra, R., Malhotra, B.D., Grover, S.K., 2000. Analytica Chimica Acta 414 (1–2), 43–50.
Lambert, T.N., Chavez, C.A., Hernandez-Sanchez, B., Lu, P., Bell, N.S., Ambrosini, A., Friedman, T., Boyle, T.J., Wheeler, D.R., Huber, D.L., 2009. Journal of Physical Chemistry C 113 (46), 19812–19823.
Li, J.H., Zhang, Z., Xu, S.F., Chen, L.X., Zhou, N., Xiong, H., Peng, H.L., 2011. Journal of Materials Chemistry 21 (48), 19267–19274.
Li, J.L., Bao, H.C., Hou, X.L., Sun, L., Wang, X.G., Gu, M., 2012. Angewandte Chemie—International Edition 51 (8), 1830–1834.
Li, X.S., Cai, W.W., An, J.H., Kim, S., Nah, J., Yang, D.X., Piner, R., Velamakanni, A., Jung, I., Tutuc, E., Banerjee, S.K., Colombo, L., Ruoff, R.S., 2009. Science 324 (5932), 1312–1314.
Li, Y.F., Bai, H.Y., Liu, Q.A., Bao, J.C., Han, M., Dai, Z.H., 2010. Biosensors and Bioelectronics 25 (10), 2356–2360.
Liu, J., Rinzler, A.G., Dai, H.J., Hafner, J.H., Bradley, R.K., Boul, P.J., Lu, A., Iverson, T., Shelimov, K., Huffman, C.B., Rodriguez-Macias, F., Shon, Y.S., Lee, T.R., Colbert, D.T., Smalley, R.E., 1998. Science 280 (5367), 1253–1256.
Liu, J.Q., Tang, J.G., Gooding, J.J., 2012. Journal of Materials Chemistry 22 (25), 12435–12452.
Lu, C.H., Yang, H.H., Zhu, C.L., Chen, X., Chen, G.N., 2009. Angewandte Chemie—International Edition 48 (26), 4785–4787.
Manjunatha, R., Suresh, G.S., Melo, J.S., D'Souza, S.F., Venkatesha, T.V., 2012. Talanta 99, 302–309.
Mirkin, C.A., Letsinger, R.L., Mucic, R.C., Storhoff, J.J., 1996. Nature 382 (6592), 607–609.
Novoselov, K.S., Geim, A.K., Morozov, S.V., Jiang, D., Zhang, Y., Dubonos, S.V., Grigorieva, I.V., Firsov, A.A., 2004. Science 306 (5696), 666–669.
Nugent, J.M., Santhanam, K.S.V., Rubio, A., Ajayan, P.M., 2001. Nano Letters 1 (2), 87–91.
Robinson, J.T., Perkins, F.K., Snow, E.S., Wei, Z.Q., Sheehan, P.E., 2008. Nano Letters 8 (10), 3137–3140.
Sanchez, C., Julian, B., Belleville, P., Popall, M., 2005. Journal of Materials Chemistry 15 (35–36), 3559–3592.
Schedin, F., Geim, A.K., Morozov, S.V., Hill, E.W., Blake, P., Katsnelson, M.I., Novoselov, K.S., 2007. Nature Materials 6 (9), 652–655.
Shan, C.S., Yang, H.F., Han, D.X., Zhang, Q.X., Ivaska, A., Niu, L., 2010. Biosensors and Bioelectronics 25 (5), 1070–1074.
Sofo, J.O., Chaudhari, A.S., Barber, G.D., 2007. Physical Review B 75, 15.
Stankovich, S., Dikin, D.A., Dommett, G.H.B., Kohlhaas, K.M., Zimney, E.J., Stach, E.A., Piner, R.D., Nguyen, S.T., Ruoff, R.S., 2006. Nature 442 (7100), 282–286.
Tan, X.C., Ll, M.J., Cai, P.X., Luo, L.J., Zou, X.Y., 2005. Analytical Biochemistry 337 (1), 111–120.
Unnikrishnan, B., Palanisamy, S., Chen, S.M., 2013. Biosensors and Bioelectronics 39 (1), 70–75.
Veca, L.M., Lu, F.S., Meziani, M.J., Cao, L., Zhang, P.Y., Qi, G., Qu, L.W., Shrestha, M., Sun, Y.P., 2009. Chemical Communications 18, 2565–2567.
Wang, X., Zhi, L.J., Mullen, K., 2008. Nano Letters 8 (1), 323–327.
Xia, Y.N., Yang, P.D., Sun, Y.G., Wu, Y.Y., Mayers, B., Gates, B., Yin, Y.D., Kim, F., Yan, Y.Q., 2003. Advanced Materials 15 (5), 353–389.
Zeng, Q.O., Cheng, J.S., Tang, L.H., Liu, X.F., Liu, Y.Z., Li, J.H., Jiang, J.H., 2010. Advanced Functional Materials 20 (19), 3366–3372.
Zhang, Y.B., Tang, T.T., Girit, C., Hao, Z., Martin, M.C., Zettl, A., Crommie, M.F., Shen, Y.R., Wang, F., 2009. Nature 459 (7248), 820–823.